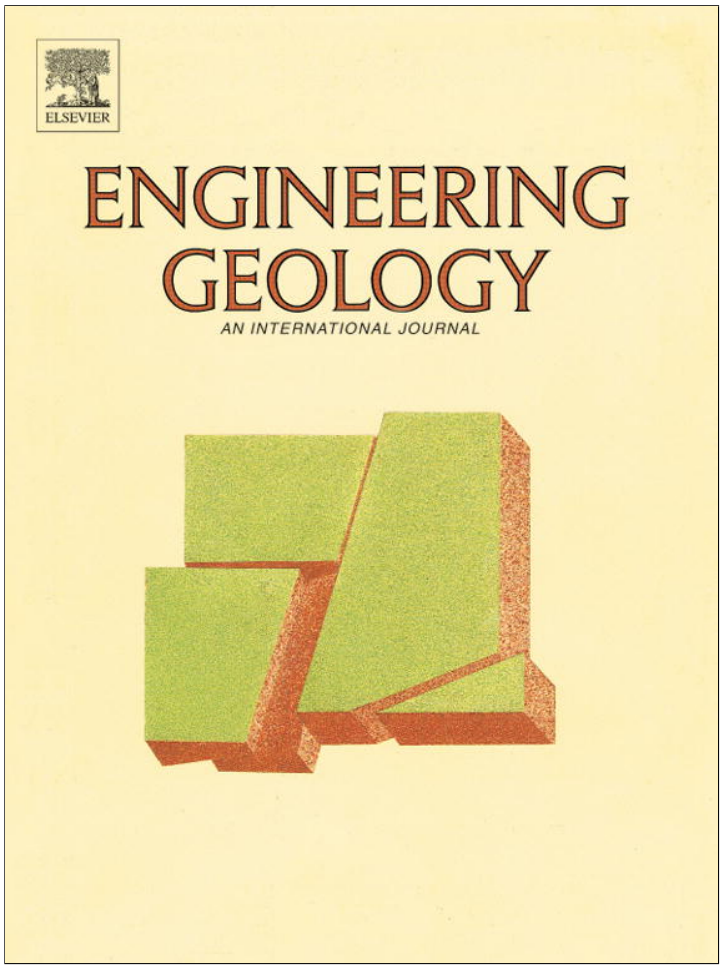

Engineering Geology 162 (2013) 22–32

Contents lists available at SciVerse ScienceDirect

Engineering Geology

journal homepage: www.elsevier.com/locate/enggeo

Infiltration-induced seasonally reactivated instability of a highway embankment near the Eisenhower Tunnel, Colorado, USA

Ning Lu [a,*], Alexandra Wayllace [a], Seboong Oh [b]

[a] Department of Civil and Environmental Engineering, Colorado School of Mines, Golden, CO 80401, United States
[b] Department of Civil Engineering, Yeungnam University, Gyeongsan, Republic of Korea

ARTICLE INFO

Article history:
Received 2 November 2012
Received in revised form 9 May 2013
Accepted 10 May 2013
Available online 20 May 2013

Keywords:
Slope stability
Unsaturated embankment
Suction stress
Infiltration-induced landslide
Factor of safety

ABSTRACT

Infiltration-induced landslides are major natural hazards. When they occur along highways they can impede traffic, damage infrastructure, and threaten public safety. This paper presents a case study of an active landslide on an embankment of Interstate-70 west of the Eisenhower Tunnel in central Colorado, USA. Records indicate that the hillslope under I-70 has moved episodically over the previous 40 years. In the previous two decades the road surface has been displaced vertically by more than 60 cm. The objective of this work is to develop a conceptual model capable of quantifying the seasonally reactivated landslide movement at the site. Inclinometer data of subsurface deformation and geologic and hydrologic mapping are used to develop the conceptual model as well as to constrain a numerical model. A two-dimensional hydro-mechanical numerical model is used to test the conceptual model under three different infiltration rates during the period of snowmelt in the spring. The framework used in the numerical model accounts for the major physical processes driving instability of the slope: time-dependent variably saturated flow, the resultant changes in stress, and induced deformation. When the snowmelt water infiltrates into the slope, the soil water content and the water-table level vary accordingly. These time-dependent variations result in changes in soil matric suction, effective stress, and consequently change in slope stability. The model calculates pore-water pressures, suction stress, and the distribution of effective stress in the embankment slope at different times. Global factors of safety as a function of time are calculated along the predetermined sliding surface using effective stresses calculated with finite elements. The slope stability assessment quantitatively confirms the conceptual model and is consistent with the displacements monitored at the site during the years of 2007–2009. It is shown that annual snowmelt infiltration of 60–100 cm of water can reduce the factor of safety by 6%, enough to sustain landslide movement for as long as 8 months each year.

1. Introduction

Infiltration-induced landslides occur worldwide and result in significant loss of life and damage to public and private properties. In the U.S., landslides occur in all 50 states and cause an estimated $1–2 billion in damage and an average of 25 fatalities each year (NRC, 2004; Godt et al., 2009). Where landslides occur along roadways and other transportation corridors, they impede traffic, damage infrastructure, and threaten public safety. Despite the significant impact of this type of geologic hazards, research to accurately forecast or prevent infiltration-induced landslides under variably saturated conditions is limited compared to the scope and size of the problem.

Traditional approaches for analyzing slope stability typically rely on limit-equilibrium methods, where the geometry of the potential failure surface in the slope is predetermined and the slope is discretized in vertical slices. In this method, the stability of each slice is analyzed using principles of force and/or moment equilibrium (e.g., Peterson, 1955; Duncan and Wright, 2005). A variety of techniques have been developed to determine stability conditions using the method of slices depending on what equations of equilibrium are included and what assumptions are made to account for inter-slice forces (e.g. Fellenius, 1936; Janbu, 1954; Bishop, 1955; Morgenstern and Price, 1965; Spencer, 1967; Sarma, 1973; Duncan, 1996; Krahn, 2003). Recent advances in analyzing slope stability employ analytical and numerical methods such as finite elements, and calculate factors of safety using either the "gravity increase method", or the "strength reduction method" (e.g. Duncan, 1996; Dawson et al., 1999; Griffiths and Lane, 1999).

Some recent studies are specifically geared to infiltration induced landslides; most of them combine an analysis of the hydrological behavior of the slope with infinite or analytical slope stability analysis or look at rainfall patterns and relate them to slope stability in large areas that include multiple landslides (e.g. Iverson, 2000; Rahardjo et al., 2001; Crosta and Frattini, 2003; Casagli et al., 2005; Tsai et al., 2008). However, most of them ignore the contribution of effective stress (suction stress)

* Corresponding author. Tel.: +1 (303) 273 3654; fax: +1 (303) 273 3602.
E-mail addresses: ninglu@mines.edu (N. Lu), awayllac@mines.edu (A. Wayllace), sebungoh@yu.ac.kr (S. Oh).

0013-7952/$ – see front matter © 2013 Published by Elsevier B.V.
http://dx.doi.org/10.1016/j.enggeo.2013.05.002

to the strength of the soil, assume full saturation conditions at the failure surface, and are restrained to shallow failures, overlooking the dynamics of groundwater table and the dependence of effective stress on transient unsaturated flow process. In recent years, slope-stability analysis has been expanded to include coupled hydro-mechanical processes under variably saturated conditions (e.g., Griffiths and Lu, 2005; Lu and Godt, 2008; Borja and White, 2010), and volumetric dilation or contraction by shearing during liquefaction and flow failures (e.g., Buscarnera and Whittle, 2012). When water infiltrates into hillslopes, the saturation of the hillslope materials and the water table level vary accordingly. Changes in the water content of the soil imply changes in gravity, matric suction, effective stress, and as a consequence, changes in stability. Thus, understanding of the physical conditions (i.e., if saturated or not) within variably saturated hillslopes when landslides occur is needed for accurate assessment and prediction.

Infiltration-induced landslides are a recurrent threat along many highway corridors, and pose a challenge to safe operation and maintenance of roadways. One of such cases is that of an active landslide located along Interstate 70 (I-70) west of the Eisenhower Tunnel, between mileposts 212.0 to 212.1 (~2 km from the tunnel), in central Colorado. The Eisenhower Tunnel crosses the continental divide and is the highest Interstate tunnel in the US. Annual surveys by the Colorado Department of Transportation (CDOT) indicate that over the past forty years, the embankment along this segment of the highway has moved episodically causing settlement of the pavement. A temporary solution has been to level the road by adding asphalt to the area of settlement; forcing at least partial closure of the roadway on several occasions. For example, in 1997 alone, five pavement overlays were placed in the area in an attempt to maintain a level road surface. Based on the asphalt thickness, settlement of about 60 cm occurred over the past two decades (Kumar, 1997; Wayllace et al., 2012). This research is part of a systematic effort to investigate this seasonally reactivated moving landslide in order to gain a sound understanding of the triggering factors for slope instability.

2. Site investigation

The study area is located about 2 km west of the west portal of the Eisenhower/Johnson Memorial Tunnel in Summit County, Colorado (Fig. 1a). The landslide is classified by the Colorado Department of Transportation (CDOT) as "large;" it has a width greater than 152 m and a depth greater than 15.2 m (Fig. 1b). Annual traffic records indicate that the average daily traffic exceeds 20,000 vehicles on this segment of I-70. Because it is located 3240 m above sea level and is surrounded by very steep terrain near the continental divide of the Rockies, the access for heavy equipment is limited. The cost to permanently remedy the situation at the site is estimated to exceed US $10 million and would necessitate closing this stretch of I-70 for an unacceptably long period.

Geologically, the area is underlain by mainly Pre-Cambrian metamorphic rocks with igneous intrusive rocks comprised of gneiss, migmatite, quartz monzonite, and pegmatites (Kumar, 1997). Three boreholes (BH1, BH2, and BH6) were drilled to depths of 20 m to 32.3 m; their locations are indicated in Fig. 1b. Bedrock is encountered at depths of 10.2 m to 21.1 m below the highway surface. According to the previous study conducted by CDOT, the geology of the slope consists of a colluvium layer that overlies decomposed gneiss, which in turn rests on intact gneiss. The fill for the road was placed directly on the colluvium layer, while a relatively thin layer of alluvium is found near the toe of the slope (Fig. 2). The groundwater table was measured at depths of 12.7 m to 20.3 m during the 1996 site investigation; it is generally parallel to the slope and is expected to vary seasonally and inter-annually based on precipitation and snowpack depth. For example, previous measurements indicate that the depth to groundwater table changed from 21.3 m to 25.4 m from July 1996 to August 1997 for borehole BH1, from 8.5 m to 9.8 m from July 1996 to July 1999 for BH2, and from 9.4 m to 15.8 m from June 1997 to July 1997 for BH6. This investigation indicates that the water table position in the embankment varies by more than 6 m at some locations. The infiltration in the slope originates mostly from the melting of a deep snowpack that accumulates in the winter months. According to the U.S. Natural Resources Conservation Service (NRCS) SNOTEL monitoring station at Summit Ranch located about 14 km from the site, the average snow depth that accumulates in the months of January through April is 107 cm, which translates into about 36 cm of snow water equivalent (SWE); however, the SWE may range from 19 cm to more than 90 cm depending on the year.

Over the past four years CDOT and Kumar and Associates, Inc. have monitored the site for ground movements. For this purpose, they installed 3 inclinometers to depths of 19.8 m and 39.0 m and information on displacement was obtained during 2007 to 2009; once the displacement exceeded the range of the inclinometers in 2009, it was not possible to further record embankment movements. Two inclinometers were installed on the east bound of I-70 while the third one was installed on the shoulder of the west bound. The inclinometers were installed so that their A-axis is along the downslope direction and the B-axis is along the I-70 road direction. Subsurface displacement was observed at depths of 10.2 m to 24.4 m with peak displacements located between 10.2 m and 16.3 m. Horizontal

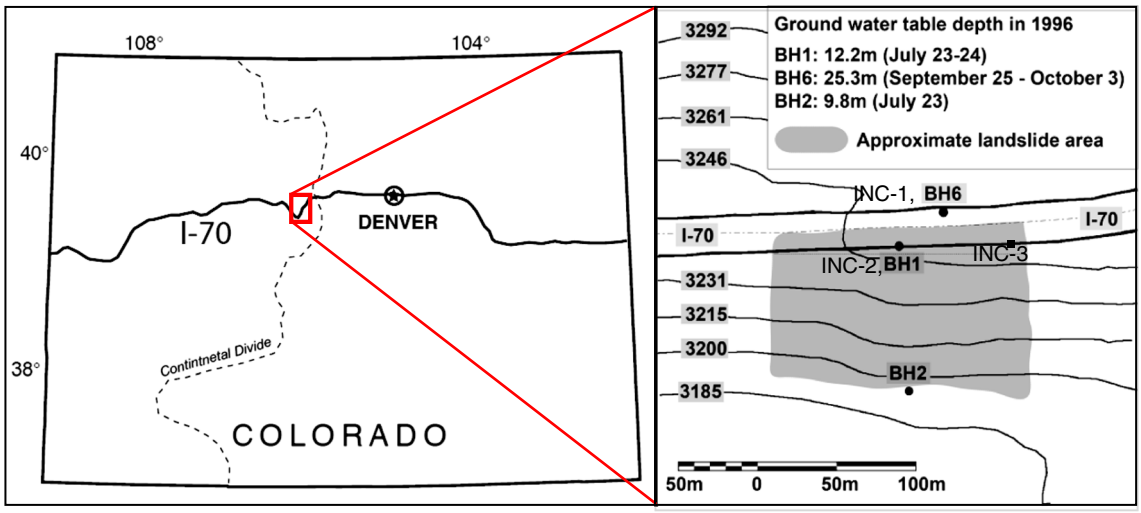

Fig. 1. The geographic location of the study site, contour map of the close-up, and displacement monitoring borehole locations.

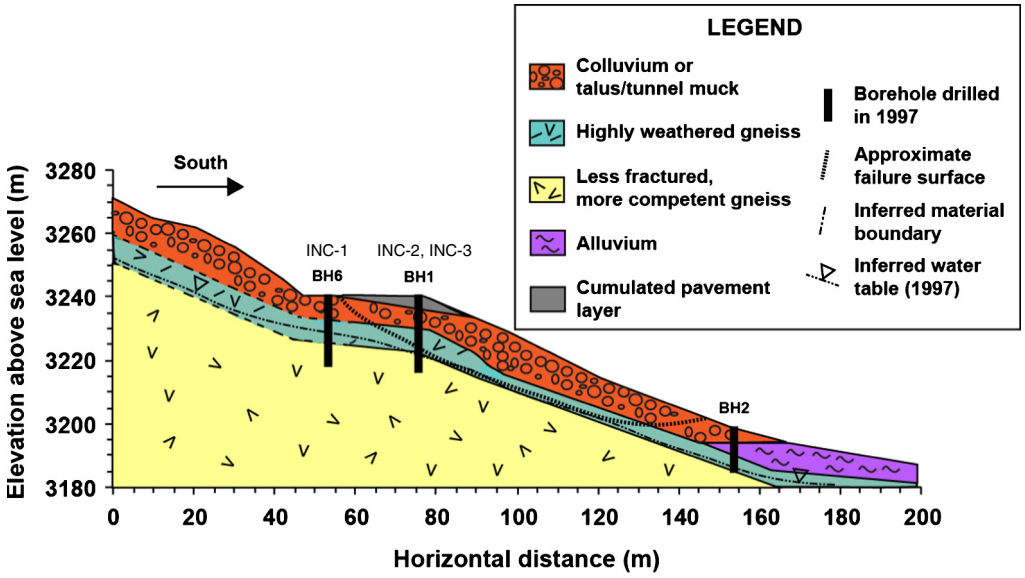

Fig. 2. Geologic cross section of the site. Borehole locations are shown as black bars.

displacements of up to 4.3 cm were recorded within one year; larger displacements were recorded during the months of June to September. Thus, the slide movement is continuous in most months of the year but accelerates during the summer season. The location of the inclinometers is marked in Figs. 1b and 2. Field observations indicate that the crown of the landslide is located between the east- and west-bound lanes of I-70 and at the toe near borehole BH2.

The displacement monitoring results for April, 2007 through October, 2009 shown in Fig. 3 (Wayllace et al., 2012) indicate that the inclinometers on the east bound of I-70 (Inc-2, Inc-3) penetrated through the sliding surface. Inclinometer data from the west bound (Inc-1) do not clearly show the location of the sliding surface, but larger displacements are observed at a depth of 12.8 m. The displacements at Inc-2 for different times are shown in Fig. 3b along the downslope direction (A-axis) and Fig. 3c along the highway direction. It is evident from the displacement data that movement is dominantly downslope. At the time of the 1996 site investigation, the water table levels at BH6, BH1, and BH2 were 25.3, 12.2, and 9.8 m below the ground surface, respectively.

3. A conceptual model for seasonally reactivated embankment sliding

Based on the above site investigations, a two-dimensional one-way coupled hydro-mechanical conceptual model is developed and is illustrated in Fig. 4. The hydro-mechanical behavior of the embankment can be conceptualized into three periods: I — snowfall accumulation, II — snow melt-shallow infiltration, and III — deep infiltration. Starting in November for Period I shown in Fig. 4a, snow starts to accumulate on the embankment. By the end of March, snow depth could be as much as 2.90 m, depending on the year. A shallow frozen zone also begins to develop in November. By the end of March, this frozen zone could be up as thick as 76 cm. The shallow frozen zone provides a dynamic hydrologic barrier for infiltration and evaporation. During this period, the water table slowly declines as a result of continuous topographically driven downslope seepage both above and below the water table. Correspondingly, the water table location slowly declines but closely mimics the position of the contact between the intact gneiss and decomposed gneiss and is likely to be at its deepest by the end of this period. Consequently, the embankment is at its most stable condition of the year and the displacement is at its minimum.

As the daily temperature rises above the freezing point beginning in April, Period II begins (Fig. 4b) and the snowpack that accumulated in Period I begins to melt at the surface. Most of the water infiltrates into the snowpack and the underlying embankment soil layer as the shallow colluvium soil is quite permeable with a saturated hydraulic conductivity of 10^{-5} m/s. Because of the increase in daily temperature in April and May, some runoff may occur. During this period, the snowmelt water infiltrates into the shallow subsurface and most annual infiltration occurs within this period. Depending on the total depth of snow on the embankment and the temperature conditions, during this period a total infiltration of as much as 90 cm is possible. Consequently, soil moisture increases and matric suction is reduced in the shallow subsurface. Depending on the location within the embankment, the infiltrated water may reach the water table and the failure surface, leading to a decrease in matric suction and increases in suction stress at this location. Most likely, the water table position during this period remains relatively unchanged. Consequently, small to moderate sliding may occur along the failure surface.

Period III continues from the previous period but surface infiltration is relatively small during time. The hydro-mechanical conditions during this period are illustrated in Fig. 4c. At the elevation of about 3240 m, summer rainstorms may occur but evaporation is most pronounced as the temperature and relative humidity are at their highest of the year. High runoff is also likely as the durations of summer storms are typically short (typically <10 min) and rainfall intensity can be high (>10 mm/min). In general, the net infiltration is relatively small in comparison with that in Period II. However, the water infiltrated during Period II continues to flow deep into the subsurface, leading to rapid rises in the water table position. Consequently, the pore-water pressure along the failure surface increases, leading to significant reduction in the effective stress and landslide motion. By the end of the summer (likely in August), the embankment is likely at its least stable condition, accompanied by high displacement rates. As the time elapses (September and October), water move into the rock below the failure surface and drains downslope resulting in a decrease in the water table position. The embankment remains at its failure state because the pore pressures both above and below the water table are still higher during this time than in the period before the snow melts.

4. A two-dimensional numerical model

4.1. A hydro-mechanical framework

In light of the above conceptual model, a transient two-dimensional numerical model was set up to quantify the groundwater conditions

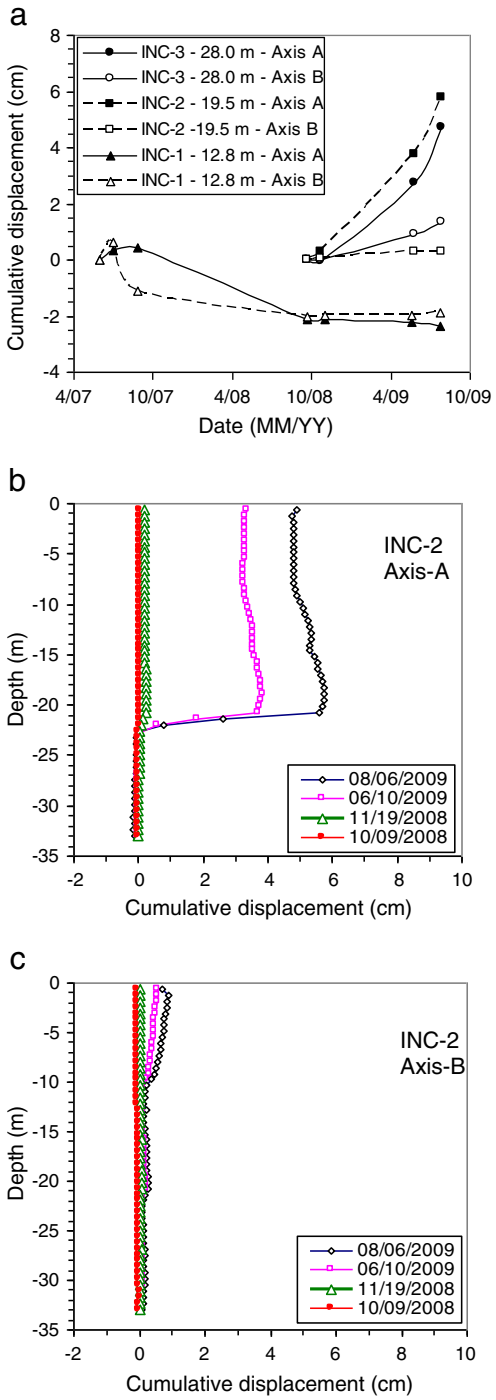

Fig. 3. Displacement data from inclinometers: (a) at the point of the largest displacement as a function of time for INC-1, INC-2, and INC-3 (A-axis is along the downslope direction, and B-axis is along I-70 road direction), (b) for INC-2 along A-axis, and (c) INC-2 along B-axis.

and stability of the I-70 embankment landslide. The model implements a rigorous, yet simple one-way coupled hydro-mechanical framework that accounts for the major physical processes in the slope: stress, deformation, and variably-saturated flow. In this framework, effective stress distributions used for the stability analysis are calculated throughout the slope by taking into account the slope's geomorphology, its hydrology, and the stress, strain, and deformation. The transient hydrological and mechanical behavior of the slope is analyzed by coupling Richards' equation with classical linear elasticity equations. The Richards' eq. is (e.g., Freeze and Cherry, 1977; Lu and Likos, 2004):

$$\nabla \cdot K(h)\nabla H + W = \frac{\partial \theta(h)}{\partial t} \tag{1}$$

where $K(h)$ is hydraulic conductivity function, h is pressure or suction head, H is total head ($H = h + z$), W is flux from a source or to a sink, and $\theta(h)$ is volumetric moisture content function commonly called the soil–water retention curve. In general, $K(h)$ and $\theta(h)$ are nonlinear functions of pressure head h.

The total stresses in the slope are mainly affected by the geometry of the slope and the hillslope material's self-weight. The governing equations for the total stresses are from balance of linear momentum:

$$\nabla \cdot (\boldsymbol{\sigma}) + \frac{\gamma}{g}\mathbf{b} = 0 \tag{2}$$

where $\boldsymbol{\sigma}$ is stress tensor with 6 stress variables in three-dimensional space, and $\mathbf{b}$ is the vector of body forces with 3 components, γ is the moist unit weight of slope materials, and g is the acceleration due to gravity. In the current hydro-mechanical framework, the coupling of Eqs. (1)–(2) is in a one-way fashion; only the solution of Eq. (2) depends on the solution of Eq. (1) as the unit weight varies with time.

The effective stress depends on the solutions of Eqs. (1)–(2), and is commonly used in the stability analysis. For variably saturated porous materials, a generalized effective stress is employed, which is defined as (Lu and Likos, 2004):

$$\boldsymbol{\sigma}' = \boldsymbol{\sigma} - (u_a + \sigma^s)\,\mathbf{I} \tag{3}$$

where $\mathbf{I}$ is the second-order identity tensor, σ^s is the suction stress that is a characteristic function of saturation or matric suction and is expressed in a closed form for all soils (Lu and Likos, 2004, 2006):

$$\sigma^s = -(u_a - u_w) \quad u_a - u_w \le 0 \tag{4a}$$

$$\sigma^s = -(u_a - u_w)S_e \qquad u_a - u_w \ge 0 \tag{4b}$$

where $(u_a - u_w)$ is the difference between air pressure u_a and water pressure u_w and is called matric suction equal to the unit weight of soil γ times minus suction head $-h$, S_e is the equivalent degree of saturation and is equal to the degree of saturation normalized by the residual degree of saturation (e.g., van Genuchten, 1980; Lu and Likos, 2004). Using van Genuchten's (1980) model to describe the soil water retention curve, suction stress (Eq. (4b)) can be expressed as a sole function of matric suction (Lu and Likos, 2004; Lu et al., 2010):

$$\sigma^s = -\frac{(u_a - u_w)}{(1 + [\alpha(u_a - u_w)]^n)^{(n-1)/n}} \tag{4c}$$

where α and n are empirical fitting parameters in van Genuchten's soil water retention model.

Once the total stress, matric suction, and suction stress distributions throughout the slope are known, effective stress is calculated from Eq. (3), (4a), (4b) or (4c), and the stability of the slope can be calculated by taking into account the shear strength properties of the soil combined with the effective stress distribution. The transient hydro-mechanical coupling and computational algorithm are shown in Fig. 5.

The described framework allows the user to quantify the effect of changes in moisture content on effective stress distribution in the slope and thus, changes in the hillslope stability.

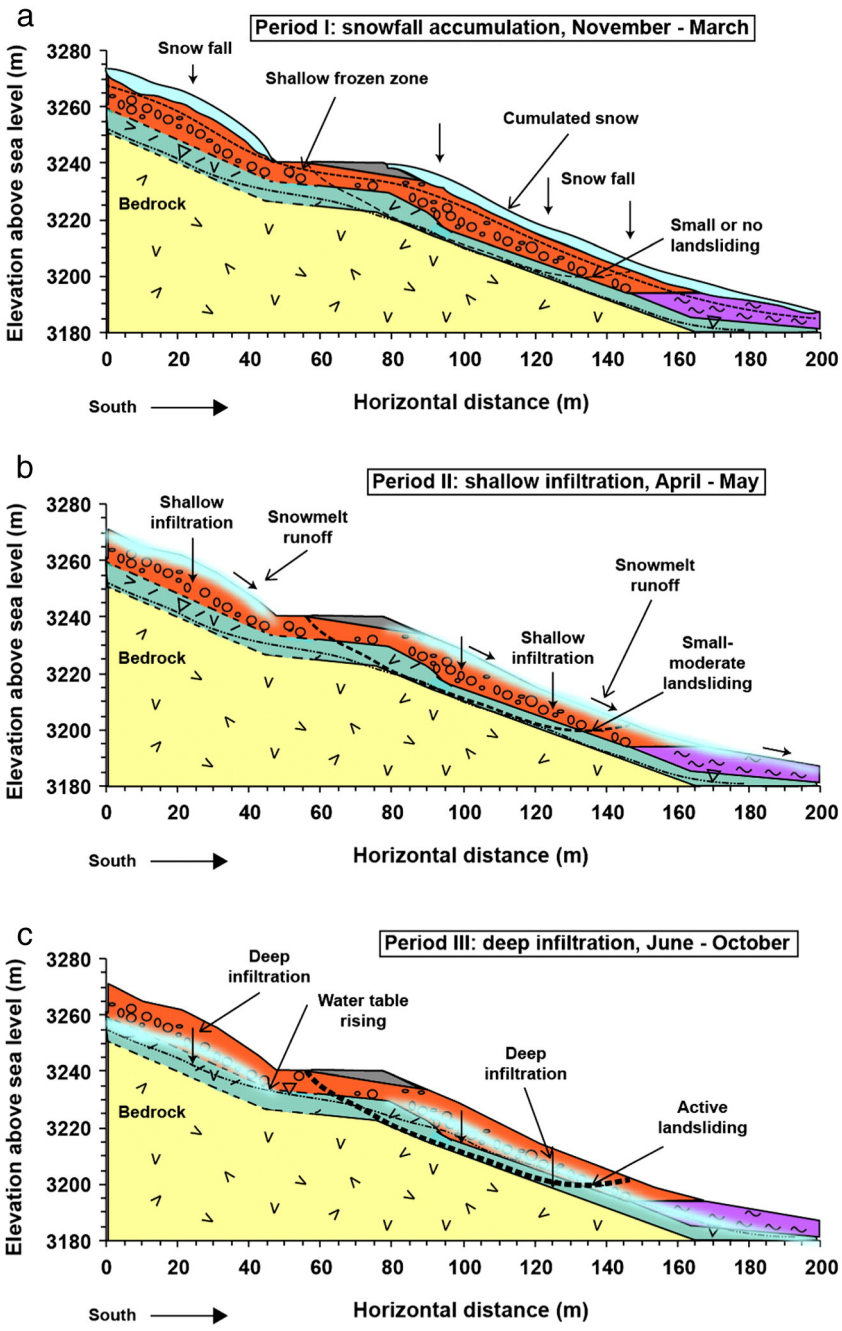

Fig. 4. A conceptual model for hydro-mechanical processes at the site.

4.2. Numerical model

The numerical model was established using the commercial slope stability software package GeoStudio, 2007 (GEO-SLOPE International, Ltd). Three modules are used to implement the coupled hydro-mechanical framework: SEEP/W to analyze the hydrological behavior of the slope (by solving Eq. (1)), SIGMA/W to calculate total stress distribution in the slope (by solving Eq. (2)), and SLOPE/W to calculate the factor of safety (by implementing Eqs. (1) to (4a), (4b), and (4c)). The first two modules use finite-element methods for stress and hydraulic head or pore water pressure (matric suction). The hydro-mechanical framework described above is applied to compute the factor of safety (FOS). In the same manner with the limit equilibrium analysis, methods of slices are used to compute the factor of safety along failure surfaces and to search a critical slip surface (a surface with the lowest FOS). The factor of safety is estimated based on stresses that are calculated by finite element analyses. Total stresses are calculated from elastic stress analysis and pore pressures and volume water contents from transient flow analysis. The stresses obtained at the integration point are projected to the nodes. At the mid-point of the slice base, the normal and shear stress are estimated as an average value of the corresponding element.

The suction stress is calculated from matric suction and moisture content by Eq. (4a), (4b), and (4c), and the shear strength is computed from effective normal stress based on suction stress as:

$$\tau_f = c' + \sigma_f' \tan\varphi' \tag{5}$$

where τ_f and σ'_f are shear stress and effective normal stress on the failure surface at failure, c' is saturated cohesion and ϕ' is saturated friction angle. In the effective normal stress, suction stress plays the identical role with pore-water pressure under saturated conditions in Terzaghi's effective stress (Eq. (3)).

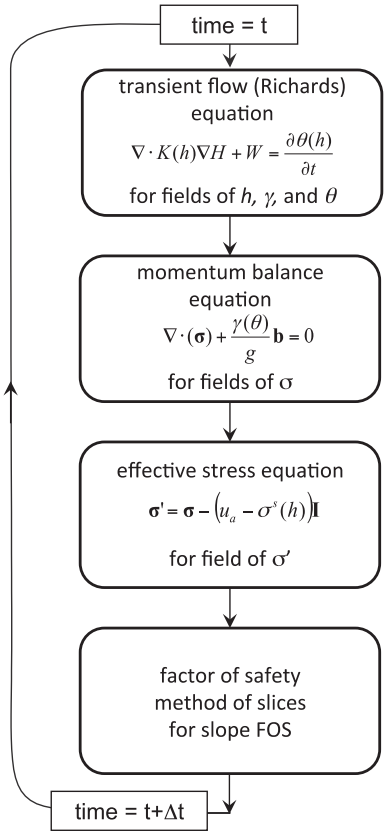

Fig. 5. A coupled hydro-mechanical framework for slope stability analysis.

The factor of safety is defined as the ratio of the mobilized and resisting shear forces and is integrated along the presumed failure surface as:

$$\mathrm{FOS} = \frac{\sum_i \left(\tau_f l_{\mathrm{base}}\right)_i}{\sum_i (\tau\, l_{\mathrm{base}})_i} \tag{6}$$

where l_{base} is the length of each slice base and i is the slice index. It should be pointed out that the FOS calculated by the method of slices defined in Eq. (6) could be greater, equal, or less than 1.0. Even though FOS is greater than 1.0, failure at the base of some local slices may already occur.

The domain, groundwater table location, and boundary conditions for the model are shown in Fig. 6. The boreholes BH1, BH2 and BH6 are shown as vertical bars and the water table levels in 1996 are shown as solid ellipses. From the geologic and hydrogeologic investigations, 5 hydrogeologic units are defined to represent the slope cross-section; their mechanical, hydrological, and strength properties are reported in Table 1. Total unit weights and strength properties for all the materials are from Kumar (1997). The hydrological properties of soils were defined using van Genuchten's model; the properties reported include the saturated volumetric water content (θ_s), the residual moisture content (θ_r), the air entry value or bubbling pressure ($u_b = 1/\alpha$), the saturated hydraulic conductivity (K_s), and the empirical parameter n. For the colluvium layer, these values were experimentally obtained using the transient water release and imbibitions method (Wayllace and Lu, 2011). Young's modulus (E) and Poisson's ratio (v) are assumed from typical values in the literature for similar materials.

The total stress and deformation distributions in the slope are simulated using SIGMA/W (solving Eq. (2) and other stress–strain and strain-displacement laws from linear elasticity theory GEO-SLOPE International, Ltd, 2007). For this module, the only load considered is the self-weight of the variably saturated embankment materials. Boundary conditions on the sides and bottom of the domain are set to zero-x (horizontal) and zero-y (vertical) displacement, respectively. The analysis assumes plane strain linear elastic conditions.

Modeling of variably saturated hydrological behavior was accomplished by setting up two analyses in SEEP/W (by solving Eq. (1)). First, initial conditions were established by doing a "steady state" analysis, where the model assumes that the boundary conditions applied are constant over time and it computes the long-term conditions. The boundary conditions specified were (Fig. 6): potential seepage face on top, with a constant flux of 6.34×10^{-9} m/section or 20 cm/year (estimated from annual precipitation data at the site), pressure heads on the sides to set the level of the water table at a depth of about 15.2 m as shown in Fig. 5, and no flow on the bottom. For each different hydrogeologic unit, the properties specified are the soil water retention curve and the hydraulic conductivity function using van Genuchten's (1980) model and Mualem's (1976) model; all materials are assumed to be isotropic. The second analysis is a "transient seepage" phase, which simulated variably saturated flow in the slope for a period of 6 years, in order to reach cyclic steady-state conditions. Boundary conditions for the sides and bottom of the domain remain identical to the ones in the "steady state" case, whereas the top boundary is set to possible seepage with a specified flux that simulates infiltration conditions in the slope for low, average, and high infiltration rates due to snowmelt. The three different infiltration rates are used to narrow the window for the plausible infiltration rate. Fig. 6b presents the flux functions for the three cases studied, where larger infiltration rates are applied for 2 months per year (when the snow melts in May and June), and "steady state" flow rate (20 cm/year) is applied the rest of the year. According to the information from the U.S. Natural Resources Conservation Service, the average snow water equivalent in the site is about 36 cm, in some years this value increases to past 90 cm and in few occasions snow water equivalent was lower than 25 cm. Thus, we apply flux rates of 30 cm/2 months, 60 cm/2 months, and 100 cm/2 months. Both the "steady state" and "transient" unsaturated flow analyses assume that the pore air pressure equals the atmospheric pressure; thus, the change in volumetric water content depends only on the change in pore-water pressure.

Slope stability is evaluated using the finite element stress-based method (SLOPE/W module), which consists of 8 steps: (1) computing the state of stress at each node, (2) using the method of slices, for the first slice find the element that is at the base-mid point of the slice, (3) computing normal and shear stress at the slice base, (4) using the calculated normal stress to compute the shear strength for the slice, (5) converting stress into forces by multiplying the values by the length of the slice, (6) repeating the process for all the slices, (7) integrating the forces over the length of the slip surface, and (8) calculating the factor of safety defined as the ratio of the available shear resistance to the mobilized shear along the predetermined slip surface. The effective stress Eqs. (3)–(4a), (4b), and (4c) are used to calculate the factor of safety. Since only linear elasticity theory is used in the analysis and no post-failure deformation and stress simulation are performed, only statically admissible solutions of Eq. (2) are computed. Therefore, a value of the factor of safety less than unity only serves as an indicator of the state of failure or landslide movement, and is not a reflection of statically inadmissible post-failure or plastic stress and deformation.

The computed pore-water pressure, volumetric water content, and suction stress values are extracted at three observation points that coincide with the measured water table locations during the 1996 site investigation in boreholes BH1, BH2, and BH6, as shown in solid ellipses in Fig. 6.

5. Quantitative confirmation of the conceptual model

The simulated distribution of pore-water pressure at the beginning of the infiltration episode (April 1) due to the 20 cm/year steady

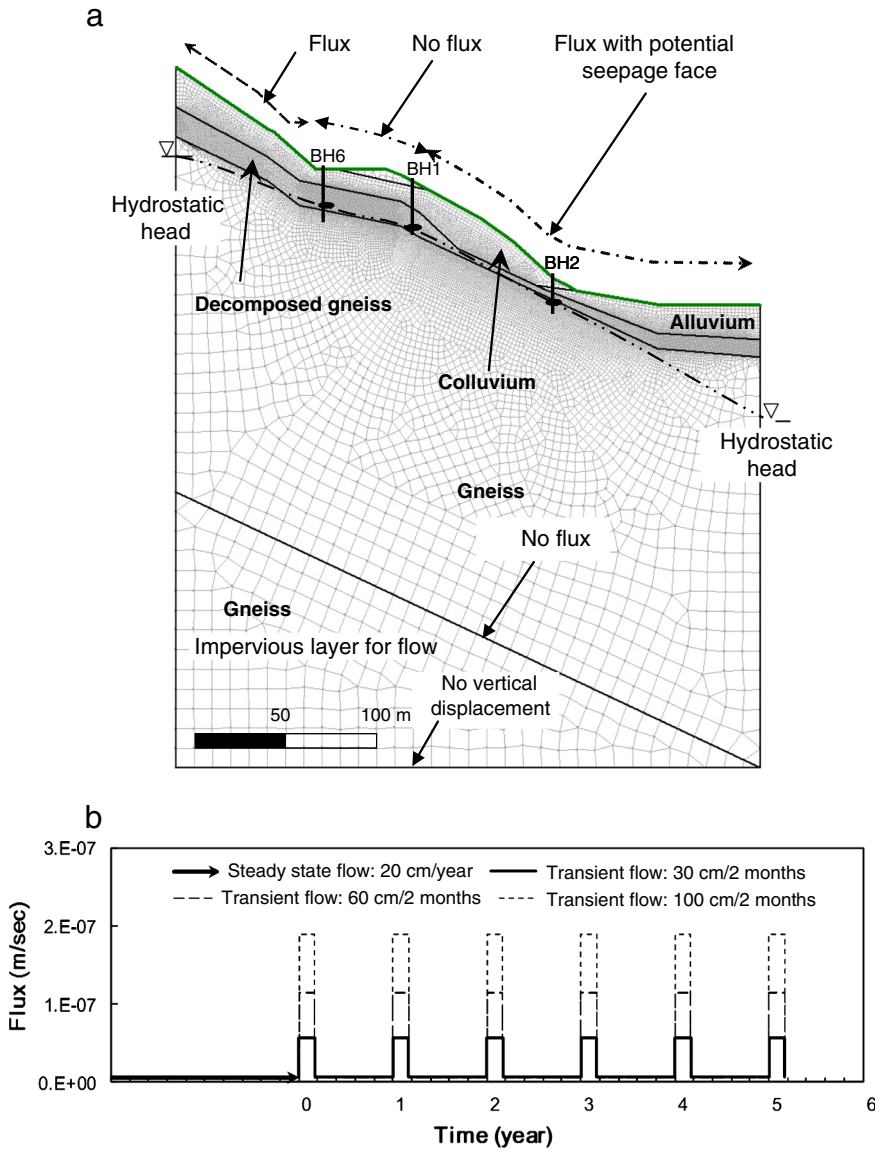

Fig. 6. Illustrations of the simulation domain: (a) initial and boundary conditions and FE mesh, and (b) the 6-year surface infiltration boundary conditions for the FE simulations.

state flow is plotted in Fig. 7a. The identified sliding surface is shown as a dashed curve. The computed water table shown as the zero-value contour closely follows the interface of the intact gneiss and decomposed gneiss. Negative pore pressure values are about −150 kPa in the crest area and close to −50 kPa in the toe area. The corresponding initial suction stress values are −100 kPa in the crest, decreasing to −25 kPa in the toe (Fig. 7b). Examples of the pore-water pressure and suction stress distributions after the average infiltration rate (60 cm/2 months) was applied for 6 years are shown in Fig. 7c–d on June 1. Under such infiltration conditions, an increase of the ground water table level is observed. During infiltration, both pore-water pressure and suction stress in the vadose zone decrease. Changes in suction stress contribute directly to changes in the effective stress field as computed by Eq. (4c).

The computed effective stress distribution is shown in Fig. 8a for the mean effective stress at the beginning of the 6-year infiltration cycles (April 1) and Fig. 8b at the 6th year of the 6-year infiltration cycles for the total 60 cm infiltration annual cycle (June 1). In general, effective stress is reduced as a result of the infiltration of snowmelt. The distribution of the reduction in effective stress or suction stress can be quantitatively assessed by subtracting the mean effective stress distribution shown in Fig. 8b from Fig. 8a, and is plotted in Fig. 8c. It can be observed that the maximum reduction in effective stress occurs above the failure surface and is up to 50 kPa beneath the slope surface south of I-70. The contours of effective stress are nearly parallel to the slope surface and the reduction diminishes as the depth increases. Along the sliding surface, the effective stress reduction is about 15 kPa.

The time-dependent pore-water pressure heads computed at the measured water table locations during the 1996 site investigation in boreholes BH1, BH2, and BH6 for the infiltration rate of 60 cm/2 months are shown in Fig. 9. Borehole BH1 is located beneath the south curb of I-70; the simulation results are shown at the contact between the decomposed gneiss and the intact gneiss. The initial value of pore-water pressure head is −1.5 m, it follows an increasing trend during the first 2 years and then displays cyclic behavior ranging from −0.4 m to 0.2 m during the last three years (Fig. 9a). The change in the effective degree of saturation corresponds to the changes in pore-water pressure head, with values ranging from 0.78 to 1.0 with the last 3 years having the lowest saturation value at 0.93 (Fig. 9b). Suction stress varies inversely in magnitude with respect to saturation and range between −3.0 kPa to 2 kPa during the last 3 years (Fig. 9c). The peak values for pore-water pressure, saturation, and suction stress show lag the end of the 2-month infiltration period by about 4 months,

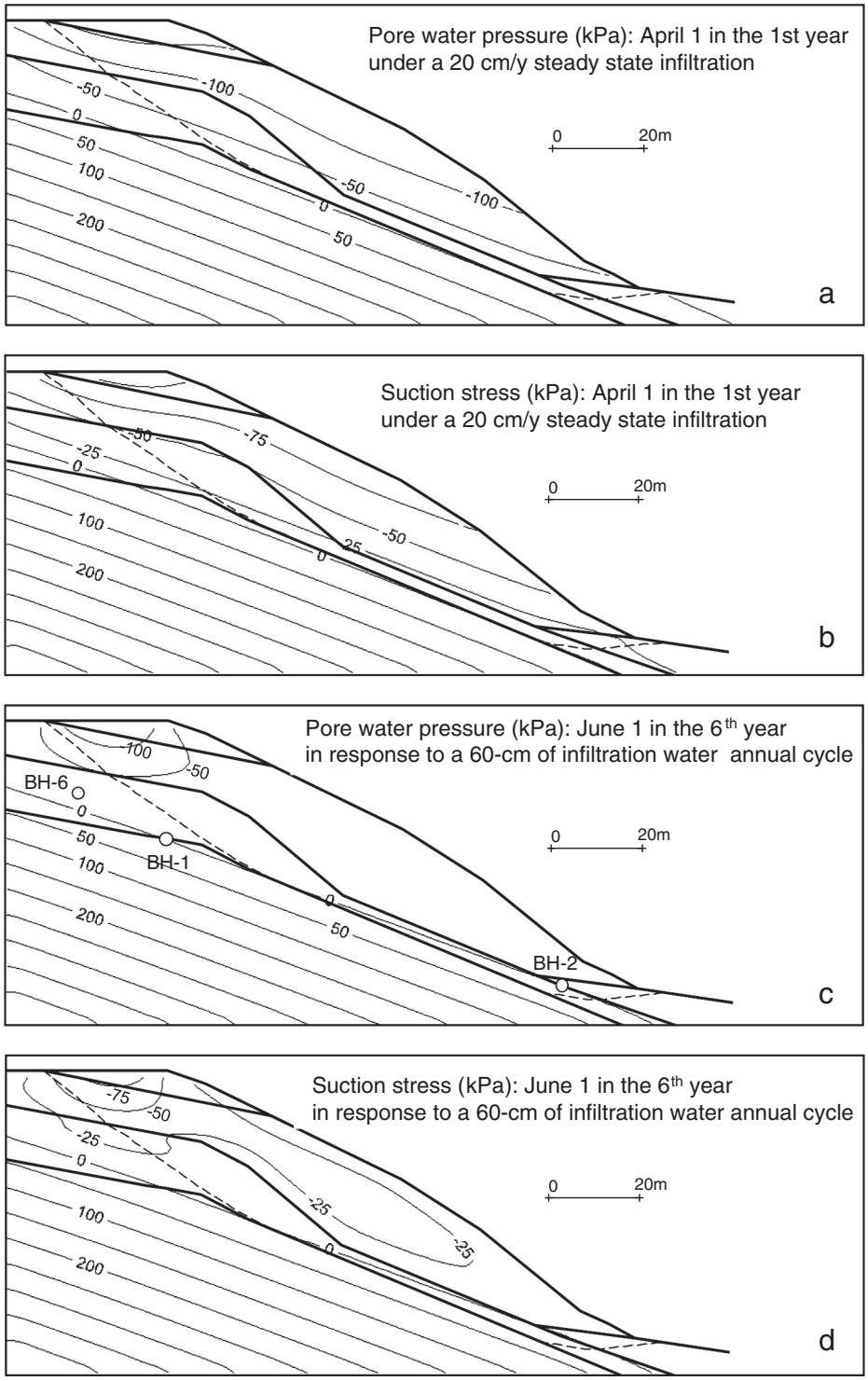

Fig. 7. Simulation results showing: (a) pore water pressure distribution at $t = 0$, (b) pore water pressure distribution at $t = 6$ years (after 6 annual cycles), (c) suction stress distribution at $t = 0$, and (d) suction stress distribution at $t = 6$ years (after 6 annual cycles).

indicating that the time for groundwater to move from the surface to the water table is about 4-months. After 3 annual cycles, the cyclic behavior of pore-water pressure, saturation, and suction stress reaches a periodic steady state. Thus the simulated transient fields of total stresses, soil moisture, matric suction, suction stress, and the water table location after 3 years are considered to be representative of conditions at the site.

Borehole BH6 is located beneath the north curb of the I-70; simulation results are shown for a location 10 m below the ground surface. The simulated patterns of pore-water pressure head, the effective degree of saturation, and suction stress are similar to BH1. Because the soil at BH6 is drier, pressure heads are more negative and suction stress values are larger in absolute terms than that at the observation point at BH1. In the last three years pressure heads in this borehole range between −3.0 to −2.6 kPa with effective saturation values of 0.72 to 0.73 and suction stress values of −28 kPa to −19 kPa.

Finally, borehole BH2 is located close to the toe of the slope. The variations in pore-water pressure, effective degree of saturation and

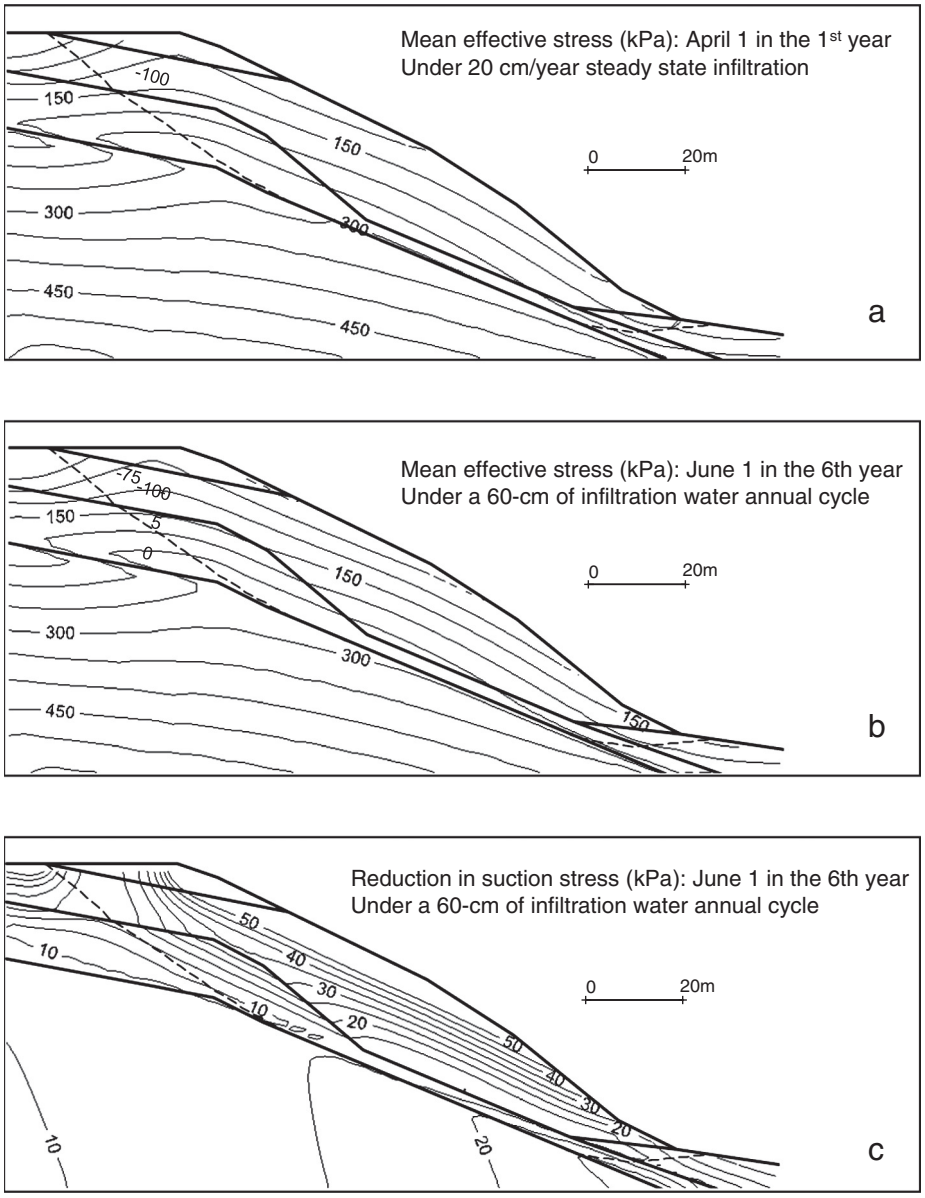

Fig. 8. Simulation results showing: (a) mean effective stress distribution at $t = 0$, (b) mean effective stress distribution at $t = 6$ years (in the 6th annual cycle) for the 60 cm/2 month infiltration rate annually, and (c) changes in mean effective stress (or changes in suction stress distribution) at $t = 6$ years (in the 6th annual cycle). The water table is above the bottom of slip surface (dashed curve). The changes in suction stress occur above the water table.

suction stress are more pronounced in this borehole, in part due to differences in material above the study point (colluvium for BH1 and BH6 and alluvium for BH2), and also due to the geometry of the slope and boundary conditions. After the periodic steady state is reached (2 years), the annual fluctuations of pore-water pressure head at this location are between −1.4 m to 0.2 m, the effective degree of saturation varies between 0.78 to 0.99, and the suction stress varies between −10 kPa and 2 kPa.

It can be drawn from the annual evolutions of pore water pressure, the effective degree of saturation, and suction stress (years 3, 4, and 5 shown in Fig. 9a–c) that the numerical model captures well the three-period conceptual model for hydro-mechanical processes in the embankment.

The factor of safety of the slope as a function of time was calculated for the three infiltration scenarios (Fig. 10a). In all three cases, the factor of safety displays a cyclic behavior so that the embankment slope is more stable when the soil is drier during the months when only the background infiltration rate of 20 cm/year is applied. Failure or FOS <1.0 is observed when the infiltration scenarios of 60 cm/2 months and 100 cm/2 months in April and May are applied. The simulated cyclic behavior of the factor of safety is consistent with the inclinometer readings; the displacement in the hillslope is not linear with time, and larger displacements correspond to periods with larger infiltration (Fig. 3). These observations also agree with the three-period conceptual model, where factors of safety less than unity are expected in the months (approximately from June to February each year) after infiltration of 60 cm/2 months or greater is imposed.

As defined in the unified effective stress principle in Eq. (3) for variably saturated materials, change in suction stress is a direct indicator of changes in effective stress ($\Delta\sigma' = -\Delta\sigma^s$ as the snow turns into water so the total stress remains relatively unchanged). Fig. 10b shows the simulated suction stress variation along the sliding surface under the three different infiltration scenarios. Initially, the sliding surface is all above the water table and suction stresses are all negative, resulting in a factor of safety of 1.054 (Fig. 10a). As the total infiltrated water increases, the lower middle portion of the slope (distance >50 m) becomes saturated, leading to positive suction stress or compressive pore-water pressures and reduction in effective stress.

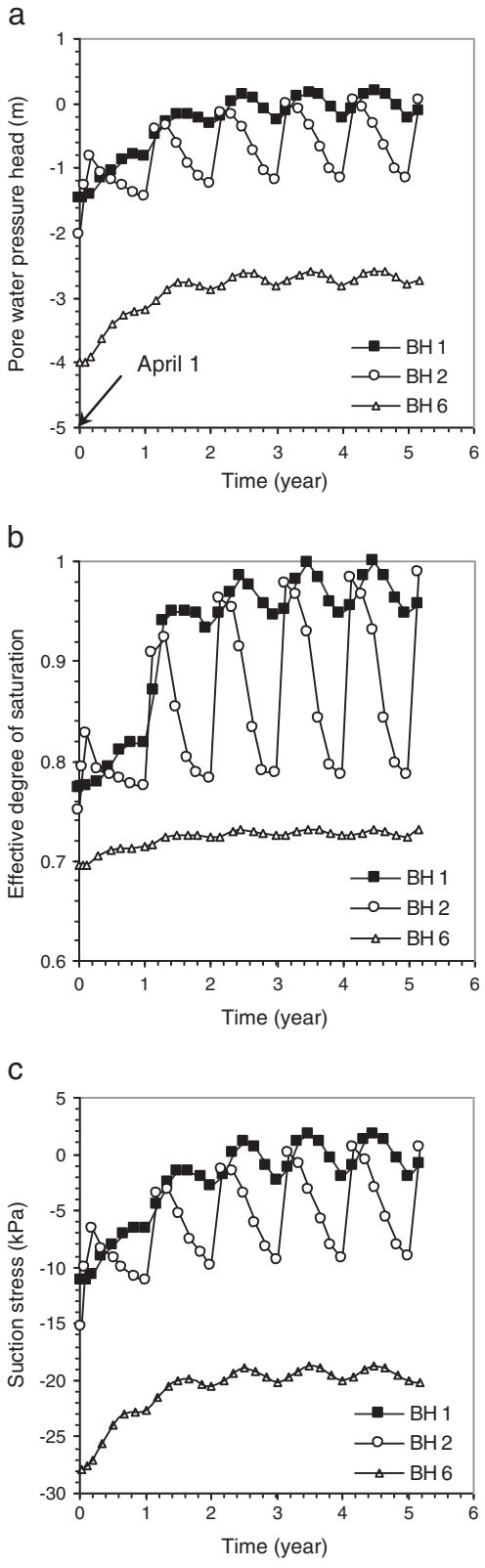

Fig. 9. Simulation results showing time-dependent variations at the 3 water table locations measured in 1996 in the 3 boreholes for: (a) pore water pressure, (b) the effective degree of saturation, and (c) suction stress.

The peak suction stress occurs about 125 m from the north boundary of the sliding surface or 25 m from the toe at the south end of the landslide body. For the 100 cm/2 month infiltration scenario, the peak pore-water pressure increase at this location is as much as 46 kPa (Fig. 10b). Thus, it appears that reducing pore-water pressure near the toe by enhancing drainage could greatly stabilize the slope, and potentially increase the factor of safety as much as 9% (the relative difference in FOS between the initial and 100 cm/2 month infiltration scenarios).

This slope-stability analysis, based on computed fields of effective stress demonstrates that suction stress variation above the water table, pore-water pressure variation below the water table due to infiltration, and the consequent cyclic water table fluctuations are responsible for the annual episodic landslide movement at the site. The annual suction stress and pore-water pressure variations along the sliding surface are on the order of 10 kPa for the 60 cm/2 month infiltration scenario, resulting in a factor of safety fluctuation between 0.99 and 1.02 with slide movement when the factor of safety of the embankment slope is equal or less than 1.00. The factor of safety varies from 0.96 to 1.0 for a 100 cm/2 month infiltration scenario. Snowmelt water in the amount >60 cm is sufficient to activate sliding a month or so after it infiltrates into the slope surface and this movement could persist year round in the 100 cm/2 month infiltration scenario. This case study illustrates that the classical slope-stability framework, commonly restrained to saturated conditions, can be readily expanded into variably saturated conditions using computed fields of suction stress. The presented coupled

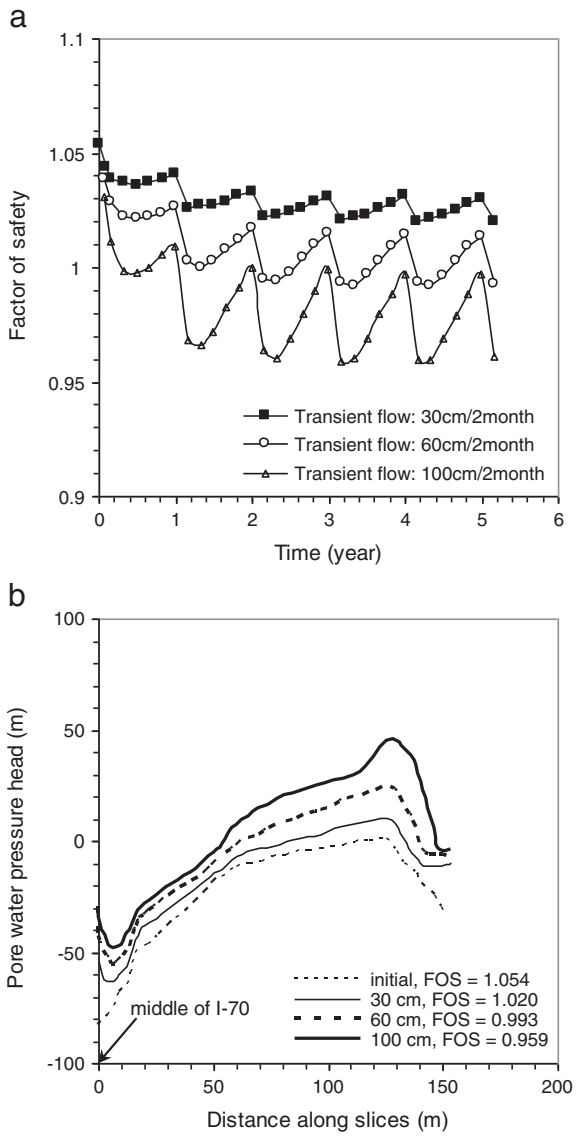

Fig. 10. Simulation results showing: (a) global factor of safety as a function of time, and (b) suction stress distribution along the failure surface.

hydro-mechanical framework is capable of quantifying and predicting the state of hillslope stability within a few percent changes in the factor of safety due to infiltration.

6. Summary and conclusions

Snowmelt- and rainfall-induced landslides are major geologic hazards worldwide that cause many fatalities and damage to property. Some of these failures occur along highways; where the need to keep roads open and in safe working condition is of particular importance. This paper presents a case study of an active landslide on an embankment of Interstate-70 west of the Eisenhower Tunnel in central Colorado, where site investigation and monitoring indicate that the hillslope under I-70 has been moving episodically during the past 40 years, with a total vertical displacement of the highway surface of more than 60 cm in the past two decades. The objective of this work is to develop a sound conceptual model capable of quantifying the seasonally reactivated landsliding at the site. Field monitoring data of subsurface deformation by inclinometers and geologic and hydrologic mapping data are used to develop a conceptual model and to constrain a numerical model. A two-dimensional hydro-mechanical numerical model was set up to test the conceptual model under three different infiltration rates during the period of snowmelt in April and May. The framework used in the model accounts for the major coupled physical processes in the slope: time-dependent variably saturated flow, and its induced stress distribution. When the snowmelt water progressively infiltrates into the slope, the soil water content and the water table level vary accordingly. These time-dependent variations result in changes in matric suction, effective stress, and consequently change in slope stability. The model calculates the distribution of pore-water pressure, suction stress, and effective stress in the embankment slope at different times. A global factor of safety along a predetermined failure surface as a function of time was calculated using finite element computed effective stresses. The following conclusions can be made.

(1) The slope stability assessment quantitatively confirms the conceptual hydro-mechanical model and is consistent with observations from the displacements monitored at the site during the years of 2007–2009.
(2) It is important to capture changes in soil moisture, soil matric suction, suction stress, and the water table location in slope stability analysis. This case study shows that under the seasonal snowmelt conditions, soil saturation can vary by 25%, matric suction can vary in several tens of kPa, the water table can vary more than 2 m, and suction stress can vary several tens of kPa in the vadose zone, leading to reactivation and deactivation of the existing landsliding.
(3) It is shown that the annual snowmelt infiltration less than 30 cm will not be sufficient to activate landslide movement but annual infiltration of 60 to100 cm of water can reduce the factor of safety of the highway embankment by 6–9%, enough to activate landsliding.
(4) The numerical modeling shows that reducing pore-water pressures near the landslide toe could greatly stabilize the slope by increasing the factor of safety as much as 9%. Thus, future remediation should consider using horizontal drainage technique as a potentially effective way for stabilizing the embankment.

Acknowledgment

This study is supported by a grant (CDOT#271001300) from the Colorado Department of Transportation to NL and AW and a grant from National Science Foundation (NSF-CMMI-0855783) to NL. In-kind support for partial field instrumentation from the Geologic Hazards Science Center of the US Geological Survey is greatly appreciated.

References

Bishop, A.W., 1955. The use of slip circle in the stability analysis of slopes. Geotechnique 5 (1), 7–17.
Borja, R.I., White, J.A., 2010. Continuum deformation and stability analyses of a steep hillside slope under rainfall infiltration. Acta Geotechnica 5, 1–14. http://dx.doi.org/10.1007/s11440-009-0108-1.
Buscarena, G., Whittle, A., 2012. Constitutive modelling approach for evaluating the triggering of flow slides. Canadian Geotechnical Journal 49 (5), 499–511.
Casagli, N., Dapporto, S., Ibsen, M., Tofani, V., Vannocci, P., 2005. Analysis of the landslide triggering mechanism during the storm of 20th –21st November 2000, in Northern Tuscany. Landslides, 3 13–21.
Crosta, G.B., Frattini, P., 2003. Distributed modelling of shallow landslides triggered by intense rainfall. Natural Hazards and Earth System Sciences 3, 81–93.
Dawson, E.M., Roth, W.H., Drescher, A., 1999. Slope stability analysis by strength reduction. Geotechnique 49 (6), 835–840.
Duncan, J.M., 1996. State of the art: limit equilibrium and finite element analysis of slopes. Journal of Geotechnical Engineering 122 (7), 577–596.
Duncan, J.M., Wright, S.G., 2005. Soil Strength and Slope Stability. John Wiley & Sons Inc, N.J., p. 309.
Fellenius, W., 1936. Calculation of the stability of earth dams. Transactions of the 2nd Congress on Large Dams, Washington, D.C., 4, pp. 445–463.
Freeze, R.A., Cherry, J.A., 1977. Groundwater. Prentice-Hall, Eaglewood Cliffs, New Jersey, p. 604.
GEO-SLOPE International, Ltd, 2007. GeoStudio (Calgary, Alberta, Canada).
Godt, J.W., Baum, R., Lu, N., 2009. Can landslides occur under unsaturated soil conditions? Geophysical Research Letters 36. http://dx.doi.org/10.1029/2008GL035996 (L02403).
Griffiths, D.V., Lane, P.A., 1999. Slope stability analysis by finite elements. Geotechnique 49 (3), 387–403.
Griffiths, D.V., Lu, N., 2005. Unsaturated slope stability analysis with steady infiltration or evaporation using elasto-plastic finite elements. International Journal for Numerical and Analytical Methods in Geomechanics 29, 249–267.
Iverson, R.M., 2000. Landslide triggering by rain infiltration. Water Resources Research 36 (7), 1897–1910.
Janbu, N., 1954. Applications of composite slip surfaces for stability analysis. Proceedings of the European Conference on the Stability of Earth Slopes, Stockholm, 3, pp. 39–43.
Krahn, J., 2003. The 2001 R.M. Hardy Lecture: the limits of limit equilibrium analyses. Canadian Geotechnical Journal 40, 643–660.
Kumar, 1997. Progress Report of Geological and Geotechnical Data Acquisition, Embankment Slope Instability Study, Straight Creek, Interstate-70 West of Eisenhower Tunnel, Summit County, Colorado. Colorado Department of Transportation, Denver, CO.
Lu, N., Godt, J.W., 2008. Infinite slope stability under unsaturated seepage conditions. Water Resources Research 44. http://dx.doi.org/10.1029/2008/WR006976 (W11404).
Lu, N., Likos, W.J., 2004. Unsaturated Soil Mechanics. John Wiley and Sons, New York 417–493.
Lu, N., Likos, W.J., 2006. Suction stress characteristic curve for unsaturated soils. Journal of Geotechnical and Geoenvironmental Engineering 132 (2), 131–142.
Lu, N., Godt, J.W., Wu, D.T., 2010. A closed-form equation for effective stress in unsaturated soils. Water Resources Research 46. http://dx.doi.org/10.1029/2009WR008646.
Morgenstern, N.R., Price, V.E., 1965. The analysis of the stability of general slip surface. Geotechnique 15 (4), 289–290.
Mualem, Y., 1976. Hysteretical models for prediction of the hydraulic conductivity of unsaturated porous media. Water Resources Research 12 (6), 1248–1254.
National Research Council, 2004. Partnership for Reducing Landslide Risk — Assessment of the National Landslides Hazard Mitigation Strategy. National Academies Press, Washington D.C., p. 131.
Petterson, K.E., 1955. The early history of circular sliding surfaces. Geotechnique 5, 275–296.
Rahardjo, H., Li, X.W., Toll, D.G., Leong, E.C., 2001. The effect of antecedent rainfall on slope stability. Geotechnical and Geological Engineering 19, 371–399.
Sarma, S.K., 1973. Stability analysis of embankments and slopes. Geotechnique 23 (3), 23–433.
Spencer, E., 1967. A method of analysis of embankments assuming parallel interslice forces. Geotechnique 17 (1), 11–26.
Tsai, T., Chen, H., Yang, J., 2008. Numerical modeling of rainstorm-induced shallow landslides in saturated and unsaturated soils. Environmental Geology 55, 1269–1277.
van Genuchten, M.Th, 1980. A closed form equation for predicting the hydraulic conductivity of unsaturated soils. Soil Science Society of America Journal 44, 892–898.
Wayllace, A., Lu, N., 2011. A transient water release and imbibitions method for rapidly measuring wetting and drying soil water retention and hydraulic conductivity functions. Geotechnical Testing Journal 35 (1), 1–15.
Wayllace, A., Lu, N., Oh, S., Thomas, D., 2012. Perennial infiltration-induced instability of Interstate-70 embankment west of the Eisenhower/Johnson Memorial Tunnels. Proceeding of GeoCongress 2012 Annual Conference. ASCE.